


 Cite this: *RSC Adv.*, 2025, **15**, 47021

## Bioactive Ti–3Cu alloys with starch, mesoporous bioactive glass nanoparticles, and clove coating for enhanced orthopedic applications

Esha Ghazanfar,<sup>a</sup> Mohsin Ali Marwat, †<sup>a</sup> Syeda Ammara Batool,<sup>b</sup> Muhammad Wajid Ullah,<sup>ce</sup> Kanwar Muhammad Adam, <sup>d</sup> Areeba Sajid<sup>a</sup> and Rimsha Areej<sup>a</sup>

Orthopedic implants, especially titanium (Ti)-based materials, are essential in treating bone and joint injuries. However, pure Ti and conventional alloys often suffer from poor bioactivity and limited osseointegration. This study investigates the synthesis of Ti–3Cu alloys, optimized through sintering at 650 °C, 750 °C, and 850 °C, and enhanced by a composite bioactive coating comprising starch, mesoporous bioactive glass nanoparticles (MBGNs), and clove particles. XRD analysis revealed the presence of the  $\alpha$ -Ti phase, with more pronounced  $Ti_2Cu$  peaks at 850 °C indicating phase formation associated with improved mechanical strength and antibacterial efficacy. Mechanical characterization showed that the substrate sintered at 750 °C exhibited the best combination of properties, with a microhardness of 91 HV and a density of 3.63 g cm<sup>-3</sup>, with porosity of 21.34%, a porosity and pore-size range known to facilitate bone ingrowth while minimizing stress shielding. The composite coating deposited via electrophoretic deposition (EPD) significantly improved surface wettability, reducing the contact angle from 133.13°  $\pm$  15.51° for the uncoated substrate to 62.67°  $\pm$  6.98° for the coated substrate. Antibacterial tests revealed the clove extracted-coated Ti–3Cu alloy exhibited moderate inhibition zones of 1.23 cm for *Escherichia coli* and 1.38 cm for *Staphylococcus aureus*. Bioactivity studies showed progressive formation of hydroxyapatite (HA), with a Ca/P ratio increasing from 1.25 on day 7 to 1.51 on day 21, indicating mature mineralization. Biodegradability testing in simulated body fluid (SBF) showed that the composite coating degraded 53.71% by day 21. Cytocompatibility tests revealed enhanced cell viability, with 104.91% cell viability on day 7 for the composite-coated substrate. These results demonstrate the Ti–3Cu alloy with composite coating, offering improved mechanical properties, antibacterial activity, bioactivity, and cellular compatibility, has potential in orthopedic applications.

Received 17th July 2025  
 Accepted 12th November 2025

DOI: 10.1039/d5ra05140a  
[rsc.li/rsc-advances](http://rsc.li/rsc-advances)

### 1. Introduction

Orthopedic implants play a crucial role in the treatment of various bone and joint injuries by restoring functionality to damaged tissues.<sup>1–5</sup> One of the primary objectives in the orthopedic implant industry is the development of materials that closely mimic the structure and function of natural bone.<sup>6</sup> Among the metals used for this purpose, titanium (Ti) and its alloys have garnered significant attention due to their superior mechanical properties, corrosion resistance, and biocompatibility.<sup>7</sup> However, the use of pure Ti and its conventional alloys is often limited by certain drawbacks, including poor bioactivity

and mechanical incompatibility with bone tissue, which can hinder osseointegration.<sup>8</sup>

The development of porous Ti alloys, particularly Ti–Cu alloys, has gained increasing interest. These alloys offer enhanced mechanical strength, resistance to corrosion, and the ability to mimic the porous structure of natural bone, which facilitates better integration with surrounding tissues.<sup>9</sup> Additionally, copper (Cu) exhibits antimicrobial activity, making it particularly suitable for orthopedic applications by preventing infections associated with implants however, more than 5% incorporation of Cu can lead to cytotoxic effects.<sup>10</sup> Importantly, literature demonstrates that the incorporation of 3% Cu in the

<sup>a</sup>Department of Materials Science and Engineering, Ghulam Ishaq Khan (GIK) Institute of Engineering Sciences and Technology, Topi 23640, Pakistan. E-mail: [mohsin.ali@giki.edu.pk](mailto:mohsin.ali@giki.edu.pk); Fax: +92-938-281032; Tel: +92-938-281026

<sup>b</sup>Materials Engineering Research Institute, Sheffield Hallam University, Sheffield, UK

<sup>c</sup>Department of Pulp & Paper Engineering, College of Light Industry and Food Engineering, Nanjing Forestry University, Nanjing 210037, China

<sup>d</sup>Faculty of Engineering and Natural Sciences, Tampere University, Tampere, FI-33014, Finland

<sup>e</sup>Department of Biosciences, University of Wah, Quaid Campus, Wah Cantt 47010, Pakistan

† These authors contributed equally to this work.



alloys, with homogeneous  $Ti_2Cu$  precipitates, can achieve >90% antibacterial rates while maintaining satisfactory mechanical strength (yield strength  $\sim 775$ –850 MPa after aging treatments). This balance of bioactivity and mechanical integrity underpins our choice of Ti-3 wt% Cu as the substrate alloy.<sup>11</sup>

In this study, we focus on the synthesis of Ti-3Cu porous alloys, using magnesium (Mg) as a space-holder agent to create the desired porosity. Mg is biodegradable and evaporates during sintering at high temperatures, leaving behind interconnected pores that promote osteoconductivity and improve the biological performance of the alloy. Moreover, the presence of porosity not only lightens the implants but also provides sites for cell adhesion, which is crucial for bone regeneration, stability, and fixation. The resulting porosity ( $\sim 21\%$ ) falls within ranges known to reduce stress shielding while still supporting structural strength and bone ingrowth.<sup>9</sup>

*Ms. Esha Ghazanfar recently completed her MS in Nanotechnology and Materials Engineering from the Ghulam Ishaq Khan Institute of Engineering Sciences and Technology (GIK Institute). She previously earned the Vice Chancellor's Gold Medal from the Institute of Space Technology (IST), Islamabad, as well as a competitive research grant from the Pakistan Engineering Council in recognition of her outstanding undergraduate work on scaffold design for orthopaedic applications. Her research interests span the synthesis of nanomaterials, nanotechnology, polymer modification, antibacterial herbal additives, biomaterials, biocomposite coatings, and scaffold engineering. With a strong academic record and a growing research portfolio, Ms. Esha aims to contribute to advancements in materials science, particularly in biomedical and nanotechnology-driven applications.*



Mohsin Ali Marwat

Dr Marwat has been serving as an Assistant Professor in the Department of Materials Science and Engineering at GIK Institute since February 2021. He has earned notable distinctions, including the Honorary International PhD Graduate title, Academic Excellence Awards for 2017–18 and 2018–19, the Excellent Volunteer Award (2018), and the Outstanding Master's Graduate Award (2017). His research spans nanomaterials, nanotechnology, energy storage materials, biomaterials, and advanced ceramics, reflected in an  $h$ -index of 29, an  $i_{10}$ -index of 45, a cumulative impact factor of  $\sim 450$ , and 2665 citations. Alongside research, he actively contributes to departmental administration, including the Board of Studies, Industrial Advisory Board, Senior Design Project coordination, and Convocation Sub-Committees. He also plays a key role in organizing the annual MTME Conference at GIK Institute. With strong academic credentials, active service, and impactful research, Dr. Marwat continues to contribute significantly to materials science and related fields.

To further enhance the biological and surface characteristics of the Ti-3Cu alloy, a multifunctional bioactive composite coating comprising starch, mesoporous bioactive glass nanoparticles (MBGNs), and clove extract was developed. Each component contributes distinct yet complementary functionalities, and their combination creates a synergistic effect essential for orthopedic applications. Starch serves as a biodegradable polymeric matrix that promotes adhesion, enables uniform particle dispersion, and provides controlled degradation. MBGNs, with their mesoporous structure and ion release capability ( $Ca^{2+}$ ,  $Si^{4+}$ ,  $P^{5+}$ ), enhance mechanical stability and stimulate hydroxyapatite nucleation, thereby supporting osteogenesis. Clove extract provides natural antibacterial and antioxidant properties, and when encapsulated within the starch-MBGNs matrix, its volatile components are released

*Dr Syeda Ammara Batool is a materials science researcher specializing in biomaterials, surface engineering, and advanced coatings for orthopedic applications. She holds a PhD (2025) and MS (2018) in Materials Science and Engineering from IST, Pakistan, and a B.Sc. in Chemical Engineering Technology from UET. Her work integrates materials synthesis, surface modification, and process optimization for biomedical applications. She is currently a KTP Associate at Sheffield Hallam University, contributing to industry-driven materials innovation. Previously, she served as a Research Assistant at IST, working on implant coatings, nanoparticle synthesis, and material characterization. She has multiple publications and reviews for leading scientific journals.*



Muhammad Wajid Ullah

Muhammad Wajid Ullah is currently working as Professor at Nanjing Forestry University, Nanjing, China. He obtained a Ph.D. degree in Chemical Engineering from Kyungpook National University, Daegu, South Korea. To date, he has published more than 195 articles in well-reputed international journals such as *Progress in Materials Science* (IF: 40.0), *Advanced Composites and Hybrid Materials* (IF: 21.8), *Materials Science & Engineering R: Reports* (IF: 26.8), *Carbohydrate Polymers* (IF: 12.5), and others, with cumulative Impact Factor  $>1500$ . In addition, he has edited 02 Books, authored 40 Monographs, and registered 02 Authorized Patents. His research has been cited  $>12,000$  Times ( $h$ -index: 63), with research interests including the fabrication of functional biomaterials via 3D Printing, Advanced cell-free enzyme systems, and physico-chemical approaches for the engineering of skin, bone, and other tissues, as well as applications in Drug Delivery, Biosensing, and Food Packaging.



gradually, extending its activity over time. This synergistic system simultaneously enhances bioactivity, antibacterial resistance, and coating stability without compromising structural integrity. The choice of coating components is crucial for improving the overall implant performance. Starch, a biopolymer, is known for enhancing the biodegradability and adhesion properties, serving as a matrix for uniform distribution of mesoporous bioactive glass nanoparticles (MBGNs) and clove particles on the substrate surface.<sup>12</sup> Although starch can swell and clove can degrade rapidly in aqueous conditions, the incorporation of MBGNs forms an inorganic network that limits excessive water absorption and prevents volatile loss of clove, improving long-term stability. This composite design also prevents accelerated corrosion of the Ti-3Cu substrate, as MBGNs buffer local pH and protect the underlying alloy. These coatings have the potential to improve the ability of alloy to promote bone regeneration and integration.<sup>13</sup>

Several studies have explored the deposition of bioactive coatings on Ti-based implants to enhance their biological properties.<sup>14</sup> A literature review revealed key findings regarding the impact of coating materials and deposition techniques on implant bioactivity and mechanical performance. For example, Tao *et al.* synthesized porous Ti-3Cu alloys at different sintering temperatures for biomedical applications, demonstrating that the incorporation of Cu helped suppress bacterial growth.<sup>15</sup> In another study, Prabakaran *et al.* deposited a composite coating of

hydroxyapatite (HA), starch, and clay which is quite similar to ours on Ti substrate using electrophoretic deposition (EPD). The coated substrate exhibited a more negative surface charge, improved biodegradability, and enhanced osteoblast viability, differentiation, and calcium mineralization, although the antibacterial activity was compromised in that study.<sup>16,17</sup> Maciag *et al.* demonstrated that MBGNs combined with zein coatings on Ti alloys, deposited through EPD, were able to form an HA layer when immersed in simulated body fluid (SBF), indicating their bioactive potential.<sup>18</sup> Ahmed *et al.* used EPD to deposit a clove-zein coating on 316L stainless steel, showing that the coatings improved hydrophilicity, adhesion, and antibacterial activity through the sustained release of eugenol from the clove particles.<sup>19,20</sup> However, the use of stainless steel substrates may lead to ion release and local inflammation after coating degradation, whereas Ti-3Cu offers superior biocompatibility and corrosion resistance, making it a safer and more durable choice.

This study aimed to synthesize Ti-3Cu alloy substrates for orthopedic applications by optimizing the sintering temperatures. We identified the 750 °C condition as optimal, offering a Ti<sub>2</sub>Cu-containing structure with balanced mechanical and porosity characteristics suitable for orthopedic implantation. A composite coating consisting of starch, MBGNs, and clove particles was deposited on the Ti-3Cu alloy sintered at 750 °C via electrophoretic deposition (EPD) at 3.5 V for 5 min, a parameter set selected from preliminary trials showing uniform coverage without agglomeration. The deposited coating was characterized to assess the distribution of particles, surface roughness,



**Kanwar Muhammad Adam**

*Kanwar Muhammad Adam is a Doctoral Researcher at Tampere University, Finland, working in the field of sustainable energy storage materials. He holds a master's degree in Materials Engineering from the Ghulam Ishaq Khan Institute of Engineering Sciences and Technology (GIKI), Pakistan. His research focuses on the design, synthesis, and electrochemical evaluation of advanced carbon-based materials, including biochar-derived*

*activated carbons and high-performance metal-organic frameworks (MOFs), metal oxides, layered double hydroxides (LDH) for high-performance supercapacitors. His work integrates green activation strategies, printable electronics, and nanomaterial engineering to develop scalable, environmentally friendly supercapacitor technologies.*

**Areeba Sajid:** Areeba Sajid received her B.S. in Chemistry from the University of Education, Lahore (Attock Campus), and her M.S. in Materials Science and Nanotechnology from Ghulam Ishaq Khan Institute of Science and Technology, Topi. Her research focuses on energy storage devices, particularly supercapacitors. She has published her work at MTME 2025 and was awarded first place in the Three-Minute Thesis Competition at ICET 2024.



**Rimsha Areej**

*Rimsha Areej is currently pursuing her master in Materials Science and Nanotechnology at the Ghulam Ishaq Khan Institute of Engineering Sciences and Technology (GIKI), Khyber Pakhtunkhwa, Pakistan. She holds a Bachelor of Science in Materials Science and Engineering from the Institute of Space Technology (IST), Islamabad, where she was awarded the Gold Medal for her outstanding final-year research project. Her research experience spans biomaterials, polymer-based additive manufacturing, scaffold engineering, and electrophoretic deposition, with multiple manuscripts under revision in reputed international journals. She previously served as a Research Assistant at Bioengineering Research & Private Limited, contributing to the development of hydrogels, orthopedic implants, and advanced 3D-printed biomedical constructs, alongside extensive material and biological characterization. She has shown her work at national and international conferences, earning distinctions and continues to build a strong multidisciplinary profile marked by scientific rigor, innovation, and commitment to advancing biomedical materials research.*



adhesion quality and biological properties. The *in vitro* antibacterial activity of the coating was assessed by measuring inhibition zones against *Escherichia coli* and *Staphylococcus aureus*.<sup>21</sup> The

coated substrates were also evaluated for bioactivity and biodegradability.<sup>22</sup> Finally, the prepared samples were evaluated for *in vitro* cytocompatibility.<sup>23</sup> The developed system is specifically

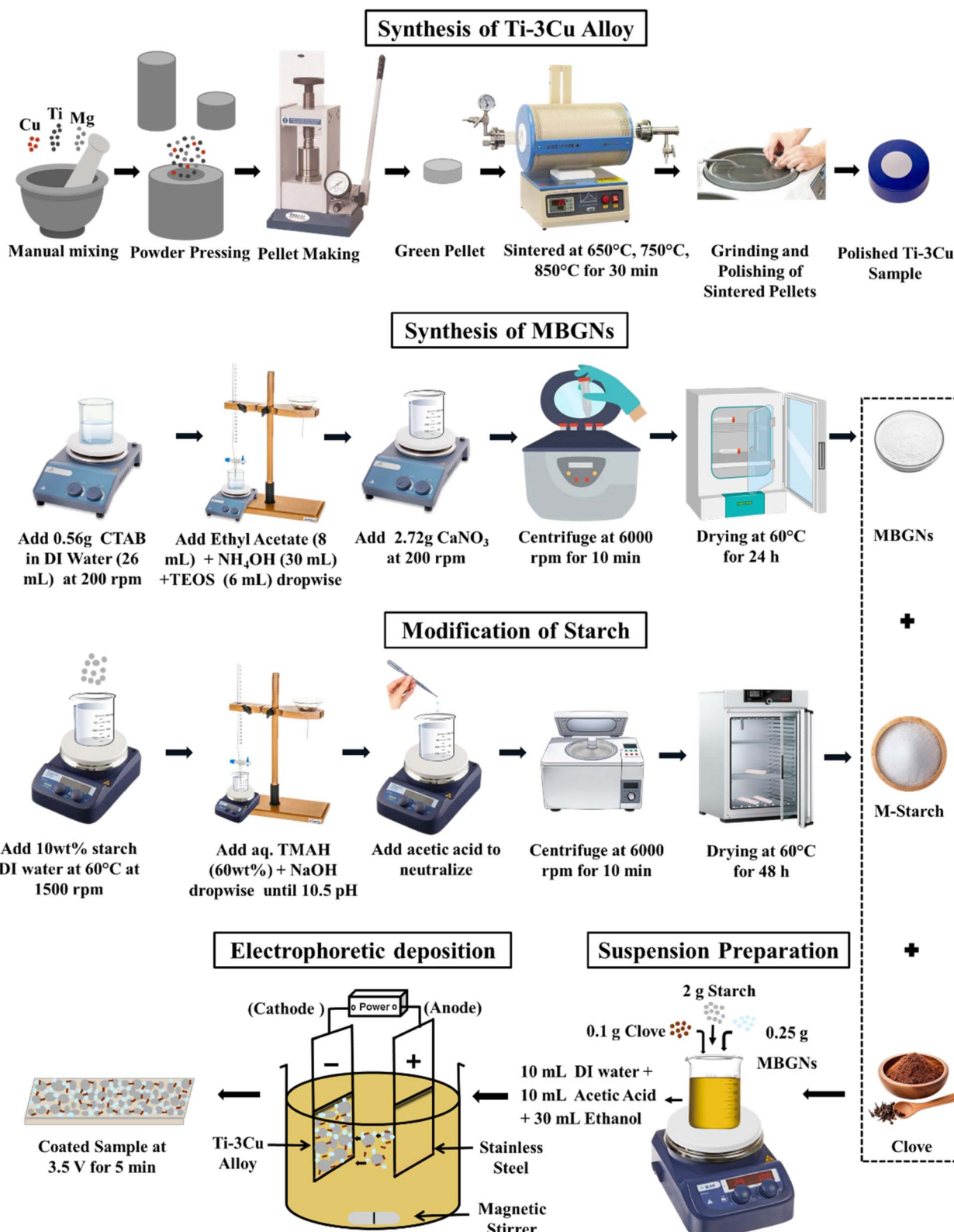


Fig. 1 Schematic illustration of the synthesis of Ti–3Cu substrate and MBGNs. The process involves the preparation of suspension, followed by the deposition of M-starch/MBGNs/clove over the Ti–3Cu substrate through electrophoretic deposition (EPD).

intended for load-bearing orthopedic implants, such as bone fixation plates and porous scaffolds, where controlled degradation, osteointegration, and infection prevention are vital for long-term performance. The results demonstrate that combining a moderately porous, mechanically robust Ti-3 wt% Cu substrate with a novel multi-component starch/MBGN/clove coating yields enhanced wettability, antibacterial function, HA deposition, and cytocompatibility, suggesting a promising approach for orthopedic implant materials.

## 2. Materials and methods

### 2.1 Materials

Titanium powder, copper powder, and magnesium powder were purchased from Sigma-Aldrich (St. Louis, MO, USA). Clove powder was sourced from Ali Express. Other chemical including ethyl acetate (99.5%), tetraethyl orthosilicate (99%, TEOS), ammonia solution (33%, NH<sub>4</sub>OH), hexadecyltrimethylammonium bromide (98%, CTAB), calcium nitrate tetrahydrate (CaNO<sub>3</sub>·4H<sub>2</sub>O), starch, tetramethylammonium hydroxide solution (25 wt% in H<sub>2</sub>O, TMAH), acetic acid (99.8%), and ethanol (>99%) were purchased from Sigma-Aldrich (St. Louis, MO, USA).

### 2.2 Preparation of porous Ti-3Cu alloys

Porous Ti-3Cu porous pellets were prepared using powder metallurgy, as reported previously.<sup>15</sup> Briefly, Ti and Cu powders were weighed in a 97 : 3 weight ratio and manually blended using a motor and pestle for 1 h. Subsequently, 5 wt% Mg powder was added as a space-holder agent and mixed for an additional 30 min. The resulting Ti-3Cu-5Mg powder mixture was compacted into green pellets using uniaxial pressure at 570 Bar for 5 min. The green compacts were placed in an alumina crucible, sealed inside a quartz tube within a vacuum tube furnace, and insulated with fiber cotton. After securing the setup, a vacuum was applied, and argon gas was introduced. The samples were sintered using microwave heating at a rate of 10 °C min<sup>-1</sup> to target temperatures of 650 °C, 750 °C, and 850 °C, each held for 20 min. The samples were then furnace-cooled to room temperature. Following sintering, the samples were mounted, then ground and polished in preparation for the EPD process. A schematic illustration of the synthesis of porous Ti-3Cu and Ti-3Cu-5Mg alloys is shown in Fig. 1.

### 2.3 Synthesis of MBGNs

Mesoporous bioactive glass nanoparticles (MBGNs) were synthesized using the Stober's process.<sup>24</sup> First, 2.24 g of CTAB was added to 104 mL of deionized water (dH<sub>2</sub>O), and the mixture was stirred at 200 rpm for 30 min at 30 °C. Once a foamy appearance developed, the heat was turned off, and 32 mL of ethyl acetate was added at room temperature, resulting in a clear solution. The pH of the solution was adjusted to 9.2 using NH<sub>4</sub>OH solution. Thereafter, 5.21 g CaNO<sub>3</sub> was added to the solution followed by dropwise addition of 23.04 mL TEOS, and the mixture was stirred for 4 h. The suspension was left overnight and then centrifuged at 6000 rpm for 10 min, and the precipitate was washed with DI water and ethanol. Finally, the

particles were oven-dried at 60 °C for 24 h. A schematic illustration of the synthesis of MBGNs is shown in Fig. 1.

### 2.4 Modification of starch

To improve the solubility of starch in organic solvents, surface modification was carried out by dissolving 10 wt% starch in distilled water at 60 °C.<sup>25</sup> Once the starch was fully dissolved, the heating was turned off, and 60 wt% aqueous TMAH was added dropwise under vigorous stirring at 1500 rpm. After complete dissolution of TMAH, the pH of the solution was adjusted to 10.5 using NaOH dropwise, and the solution was left to stir for 3–4 h. Following this, the solution was neutralized by adding acetic acid and stirred for an additional 2–3 h. The resulting suspension was then centrifuged at 6000 rpm for 10 min, washed with absolute ethanol, and dried at 60 °C for 24 h to obtain the modified starch particles. A schematic illustration of the preparation of modified starch particles is shown in Fig. 1.

### 2.5 Preparation of starch/clove/MBGNs suspension

A suspension containing MBGNs, starch, and clove was used for EPD, following the composition optimized in a previous study.<sup>26</sup> First, a starch solution was prepared by dissolving 2 g starch in 10 mL DI water with continuous magnetic stirring at 300 rpm. Once the starch was gelled, 10 mL of acetic acid was added. Another solution was prepared by sequentially adding 0.1 g clove and 0.25 g MBGNs to 30 mL of ethanol, with continuous stirring to ensure proper dispersion. After 30 min of stirring, the solution was ultrasonicated for 10 min to achieve a more homogeneous mixture. Once both solutions were ready, the ethanol-based solution was added dropwise to the starch solution under continuous stirring to prevent the formation of lumps. The final mixture was stirred for an additional 3 h to form stable suspension with its pH maintained at 2.3. A schematic illustration of the preparation of suspension is shown in Fig. 1.

### 2.6 Electrophoretic deposition

Prior to EPD, the surface of the Ti-3Cu substrate was ground and polished to ensure smoothness and to remove dirt and debris. The Ti-3Cu substrate was then used as the working electrode (cathode), while a stainless-steel plate served as the counter electrode connected to a KPS6010D Wanptek DC power supply and immersed in the prepared suspension (starch, clove, MBGNs). A voltage of 3.5 V was applied, causing the positively charged particles in the suspension to migrate toward the cathode and deposit onto the Ti-3Cu substrate. The deposition process was carried out at room temperature for 5 min. These parameters were chosen based on preliminary trials that

Table 1 The yield of the deposited coating is listed below

Sample	Initial weight	Final weight	%Yield
1	2.014	2.047	1.639
2	2.064	2.098	1.647
3	2.055	2.089	1.65
<b>Avg = 1.647</b>			



produced the consistently yielded uniform and adherent coating (Table 1).<sup>27</sup> All tests were performed in triplicate and standard deviations are reported. The yield of the deposited particles was calculated using eqn (1).<sup>27</sup>

$$\text{Yield}(\%) = \frac{\text{Final weight} - \text{Initial weight}}{\text{Initial weight}} \times 100 \quad (1)$$

## 2.7 Characterization

Optical microscopy (OLYMPUS, Japan) was used to examine the porous structure of Ti-3Cu alloys. The surface morphology and elemental composition of prepared alloys, starch particles, and MBGNs were analyzed through scanning electron microscope (SEM) coupled with energy-dispersive X-ray spectroscopy (EDX, ZEISS instrument, EVO15, UK).<sup>28–30</sup> X-ray diffraction (XRD, AXRD LPD, Proto, UK) was performed to identify the phase composition of Ti-3Cu substrates sintered at 650 °C, 750 °C, and 850 °C. X-ray intensity was recorded against  $2\theta$  using CuK $\alpha$  radiation over a scanning range of 10° to 90°.<sup>31,32</sup> To further analyze the chemical composition of starch, M-starch, MBGNs, clove, and the composite-coated substrate, Fourier-transform infrared spectroscopy (ATR-FTIR, ThermoFisher Nicolet Summit Pro) was conducted. The crystal platform was cleaned with 99% ethanol, and background noise was removed using OMNIC Paradigm software. The sample was placed on the crystal with a spatula, secured using the knob, and scanned in absorbance mode.<sup>31,32</sup>

## 2.8 Microhardness and density

Microhardness testing was carried out using a Tukon hardness tester (Wilson instruments Inc., New York, USA). Briefly, 5 indentations were made on each sintered Ti-3Cu sample using a diamond indenter under a 50 g load. The sintered density and theoretical density of the sintered samples were determined using eqn (2) and (3), respectively.

$$\text{Sintered density}(\rho_s) = \frac{\text{Mass}}{\text{Volume}} \quad (2)$$

$$\text{Theoretical density}(\rho_T) = \left( \frac{\% \text{Cu}}{\rho_{\text{Cu}}} \right) + \left( \frac{\% \text{Ti}}{\rho_{\text{Ti}}} \right) + \left( \frac{\% \text{Mg}}{\rho_{\text{Mg}}} \right) \quad (3)$$

## 2.9 Surface roughness and porosity

A profilometer was used to assess surface roughness. The stylus was drawn along a 1 cm line on the coated surface, and average roughness ( $R_a$ ) was recorded.<sup>33</sup> The volume of the Ti-3Cu substrates was determined using a helium Pycnometer (InstruQuest, USA). Helium gas was used to measure the volume of the empty chamber and then the volume with the sample. The difference between the two values yielded to the actual volume of the substrate. The sample mass was measured using a precision weighing machine, and both values were used to calculate density. The porosity of sintered samples was determined using eqn (4).

$$\text{Porosity}(\%) = 1 - \frac{\rho_s}{\rho_T} \times 100 \quad (4)$$

## 2.10 Surface wettability and adhesion testing

Wettability was assessed by placing a 5  $\mu\text{L}$  drop of distilled water on both uncoated and coated Ti-3Cu substrates at five different points. After 10 s, images of the drops were captured at drop level, and contact angles were measured using ImageJ software. Adhesion strength of the coatings was evaluated *via* a cross-cut tape test according to ASTM standard D3359.<sup>34</sup> A crosshatch pattern was made using a cutter, followed by application and removal of adhesive tape. The surface was examined under an optical microscope before and after the test to assess coating removal.<sup>35</sup>

## 2.11 Antibacterial activity and *in vitro* bioactivity

The antibacterial activity of sintered samples, clove, and coated samples was measured on solid agar plates through disc diffusion assay (DDA) against *Escherichia coli* and *Staphylococcus aureus*, cultured on respective growth media. Briefly, all samples were cut into 13 mm diameter disc-shaped, freeze-dried, and sterilized. Thereafter, fresh precultures of both bacterial strains were spread on separate agar plates, and the discs were placed on top and incubated at 37 °C for 24 h. Finally, the inhibition zones were measured. To assess the bioactivity, coated substrate was immersed in 30 mL of simulated body fluid (SBF), prepared following Kokubo's protocol (pH 7.4), and incubated at 37 °C with shaking at 150 rpm for 7, 14, and 21 days (BioBase, China). After each time point, the samples were washed with distilled water, dried, and examined using SEM.<sup>36</sup>

## 2.12 Cytocompatibility testing

Cytocompatibility was evaluated using MG-63 osteoblast cells (CRL1427, ATCC, Manassas, VA) and the WST-8 assay.<sup>37</sup> Disc-shaped Ti-3Cu and M-starch/MBGNs/clove-coated samples were sterilized under UV light for 1 h and used in 24-well plates. A 316L SS was used as a control. Briefly, cells were cultured in Dulbecco's modified Eagle's medium (DMEM, Gibco) supplemented with 10% fetal bovine serum (FBS, Gibco) and 1% penicillin/streptomycin (Gibco), incubated in a CO<sub>2</sub> incubator (NUAIRE) at 37 °C until 80–90% confluence was reached. After incubation, cells were washed with phosphate-buffered saline (PBS, Gibco), detached using trypsin-EDTA (Gibco), stained with trypan blue (Sigma-Aldrich, St. Louis, MO, USA), and counted using a hemocytometer. The sterilized samples were seeded with a 10<sup>5</sup> cells per mL and incubated with at 37 °C, 5% CO<sub>2</sub>, and >85% humidity for 48 h.<sup>38</sup> Cell viability was assessed using the WST-8 assay (Cell counting Kit 8, Sigma-Aldrich, St. Louis, MO, USA). After incubation, the cell culture medium was replaced with 400  $\mu\text{L}$  fresh DMEM containing 1% WST-8 reagent. Absorbance was measured, and control samples were considered 100% viable.<sup>39</sup>

## 2.13 Statistical analysis

All experimental data are presented as mean  $\pm$  standard deviation (SD) based on three independent trials and statistically



analyzed using one-way analysis of variance (ANOVA), with significance set at  $p < 0.05$ .

### 3. Results and discussion

#### 3.1 Structural properties and mechanical strength of Ti-3Cu substrate

An X-ray diffraction (XRD) analysis was conducted to identify the phases present in Ti-3Cu substrates sintered at 650 °C, 750 °C, and 850 °C (Fig. 2A). The results revealed the dominant presence of  $\alpha$ -Ti phases at 35.3°, 38.4°, 40.4°, 53.1°, 63.2°, 70.6°, 76.3°, and 77.6° (JCPDS-ICDD, 44-1294) across all sintering temperatures.<sup>15</sup> Notably, no peaks corresponding to Mg were observed, confirming the complete evaporation of Mg, which was used as a space holder during the sintering process. This indicates the successful removal of the space holder, facilitating the formation of the porous structure. Copper diffraction peaks were also absent due to the low copper content (less than 5%).

However, the intensity of  $\text{Ti}_2\text{Cu}$  diffraction peaks increased progressively with higher sintering temperatures. At 850 °C, two distinct peaks for  $\text{Ti}_2\text{Cu}$  were observed at 39.7° and 43.4°, suggesting an increase in the  $\text{Ti}_2\text{Cu}$  phase content with the rising sintering temperature. The presence of  $\text{Ti}_2\text{Cu}$  has been reported to strengthen the substrate through dispersion hardening and improved load transfer across the  $\alpha$ -Ti matrix; however, excessive  $\text{Ti}_2\text{Cu}$  precipitation may increase brittleness, which must be carefully balanced for biomedical applications to maintain structural integrity under physiological loading.

Microhardness, density, and porosity were measured to evaluate the mechanical and structural properties of Ti-3Cu substrate sintered at 650 °C, 750 °C, and 850 °C (Fig. 2B and C). These properties are essential for assessing implant functionality and bone regeneration, as both strength and moderate porosity are crucial factors. The microhardness values showed a steady increase with higher sintering temperatures (Fig. 2B). The substrate sintered at 650 °C had a microhardness of 85 HV,

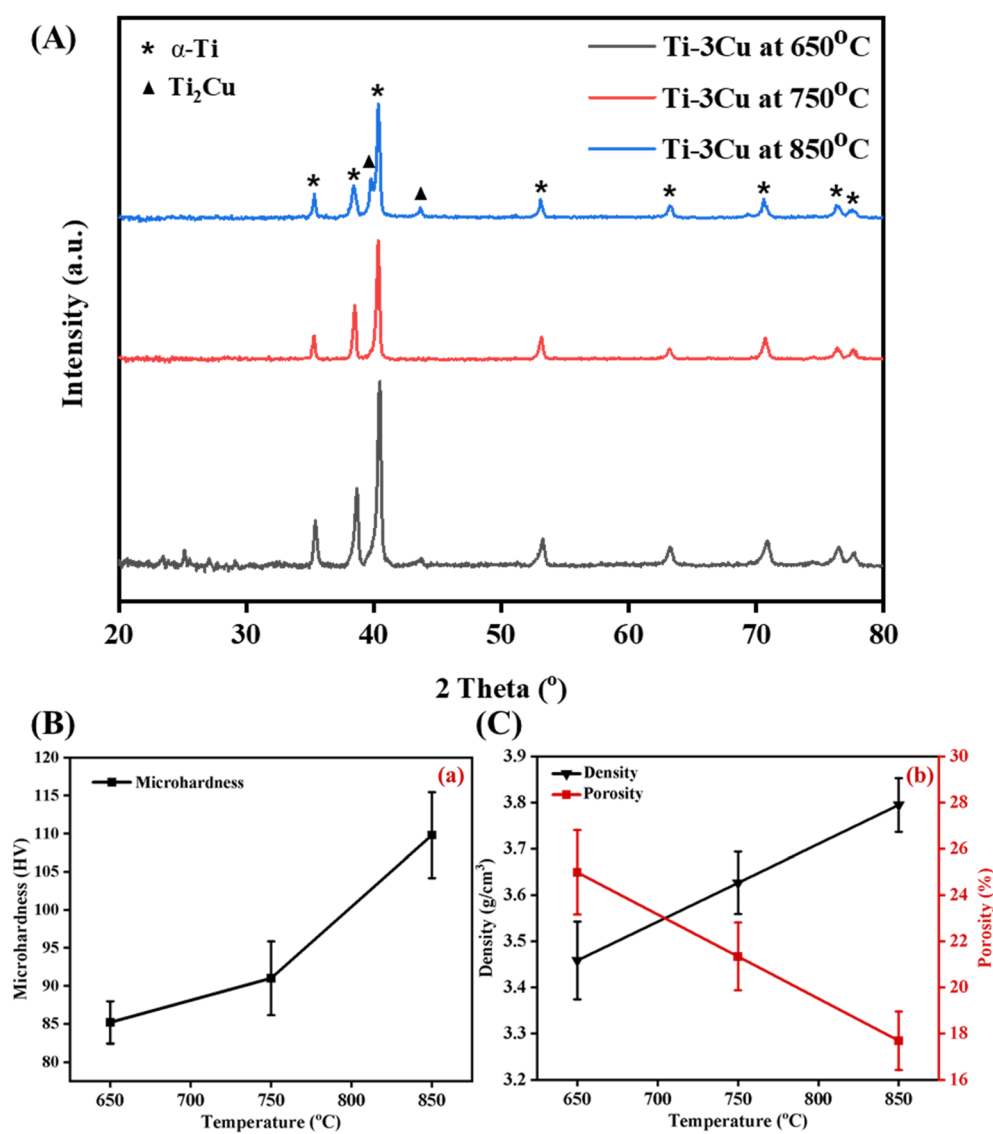


Fig. 2 (A) XRD patterns, (B) microhardness, and (C) density and porosity of Ti-3Cu substrates sintered at 650 °C, 750 °C, and 850 °C.



while the one sintered at 750 °C showed 91 HV. At 850 °C, the highest microhardness of 110 HV at 50 g was achieved, which can be attributed to the reduced porosity and enhanced densification at higher sintering temperatures. This results in a stronger structure that is more resilient to mechanical stresses.<sup>15</sup> Statistical analysis confirmed that the differences in hardness and density values across the sintering temperatures were significant ( $p < 0.05$ ). The density and porosity result further validate the trend observed in the microhardness data (Fig. 2C). At 650 °C, the substrate had a density of  $3.46 \text{ g cm}^{-3}$  and the porosity of 24.98%. When sintered at 750 °C, the density increased to  $3.63 \text{ g cm}^{-3}$ , and the porosity decreased to 21.34%. At 850 °C, the lowest porosity of 17.69% and the highest density of  $3.80 \text{ g cm}^{-3}$  were observed. These results indicate that as the sintering temperature increases, the densification of the substrate also increases, leading to lower porosity and higher mechanical strength, which is ideal for load-bearing applications. However, orthopedic implants also require interconnected pores within the ideal 100–400 μm range for bone ingrowth. At 650 °C, although pore sizes were larger, the mechanical strength was insufficient, while at 850 °C, the smaller pore sizes (<100 μm) are less favorable for osteoconduction. The 750 °C sample provided ~90 μm average pore size with interconnected morphology, a moderate porosity (~21%), and sufficient mechanical strength, offering an optimal balance between load-bearing capability and osteointegration potential. This pore structure also facilitates coating

adherence and mechanical interlocking of the M-starch/MBGNs/clove layer, enhancing long-term stability under cyclic loading.<sup>40</sup>

Optical microscopy and SEM analysis were conducted to examine the microstructure of the synthesized sintered Ti–3Cu substrates. Optical images clearly show the presence of pores, which were created using Mg as a space holder agent in the sintered substrates at 650 °C, 750 °C, and 850 °C (Fig. 3a1–a3). A notable observation is the progressive reduction in pore size with increasing sintering temperature: approximately 145 μm at 650 °C, 90 μm at 750 °C, and 55 μm at 850 °C. Specifically, the substrates sintered at 650 °C exhibited larger, interconnected pores, while those sintered at 750 °C and 850 °C showed a gradual decrease in pore size. The substrate which was sintered at higher temperatures also exhibited more distinct, well-formed pores. The reduction in pore size with increased temperature can be attributed to enhanced densification, leading to more compact substrates. Additionally, the presence of small pores, resulting from interparticle gaps, decreased as the sintering temperature increased. Importantly, interconnectivity was still preserved in the 750 °C samples, which is critical for nutrient transport and bone tissue ingrowth. Further SEM analysis, combined with EDX, was performed to confirm the presence of phases. It was confirmed that Mg was completely evaporated from the substrates.<sup>15</sup> At 650 °C (Fig. 3b1 and b2), a few white-colored particles were detected on the surface of the substrate. The number of these white particles

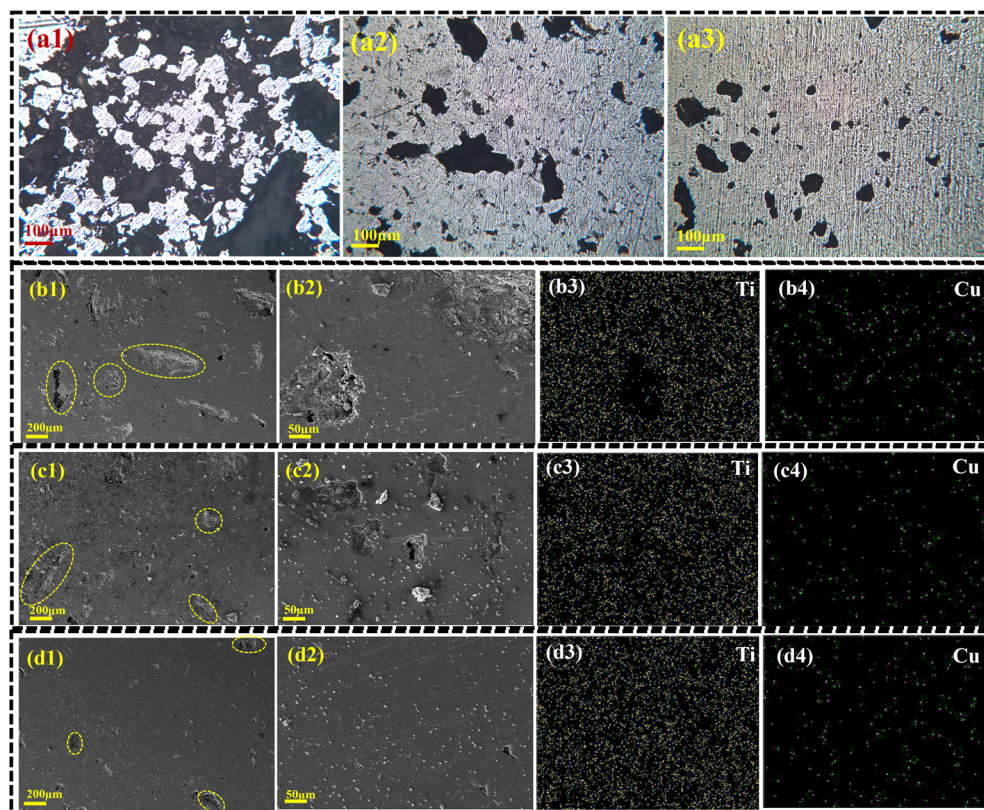


Fig. 3 Optical microscope images of Ti–3Cu substrate sintered at (a1) 650 °C, (a2), 750 °C, and (a3) 850 °C. SEM images and color mapping of Ti–3Cu substrates sintered at (b1–b4) 650 °C, (c1–c4) 750 °C, and (d1–d4) 850 °C.

increased in the substrate sintered at 750 °C (Fig. 3c1 and c2), and at 850 °C, the entire surface was covered with particles (Fig. 3d1 and d2). Color mapping of the substrates (Fig. 3b4, c4 and d4) confirmed the presence of Cu in these white particles, indicating the formation of the  $\text{Ti}_2\text{Cu}$  phase within the  $\alpha$ -Ti matrix (Fig. 3b3, c3 and d3).

### 3.2 Structural and physiological properties of coated Ti-3Cu substrate

Based on phases, microstructure, and mechanical analyses of substrates, sintered at 650 °C, 750 °C and 850 °C, the 750 °C substrate was selected for further study. The 650 °C substrate was too porous and lacked sufficient strength to support body weight, while the 850 °C substrate had a few pores and posed a risk of stress shielding due to its high strength and hardness.

Based on the SEM images, the synthesized MBGNs exhibit a uniform size distribution, with diameters ranging from 80 to 90 nm. This consistent particle size is crucial for ensuring reliable performance in orthopedic implants (Fig. 4a1 and a2). Elemental mapping further confirmed the presence of Si, Ca, and O in the MBGNs (Fig. 4a3–a5). In contrast, the SEM images of the starch particles revealed significantly larger sizes, in the micrometer range. Elemental mapping indicates the presence of C and O in these particles (Fig. 4b1–b3). The combined use of starch, MBGNs, and clove provides a synergistic multifunctional coating: starch serves as the biodegradable polymeric matrix offering strong adhesion and flexibility; MBGNs

introduce controlled ion release and bioactivity through Ca–Si–P dissolution, while clove imparts natural antibacterial and antioxidant effects. Together, these components form a mechanically stable and biologically active coating layer, where MBGNs' inorganic framework reinforces the polymer matrix, minimizing early degradation of starch or volatilization of clove and ensuring coating integrity over several weeks of physiological exposure.

SEM analysis of the M-starch/MBGNs/clove composite-coated substrate confirmed the successful and uniform deposition of the synthesized MBGNs, along with starch and clove particles, across the entire surface (Fig. 4c1). The particles were not only uniformly distributed on the surface but also penetrated into the pores of the substrate (Fig. 4c2 and c3). The coating thickness, measured from a cross-sectional image, was 13.78  $\mu\text{m}$  (Fig. 4c4). Elemental mapping of the coating substrate confirmed the presence of all expected element, Si, Ca, C, and O, indicating the successful deposition of all components (Fig. 4c5–c8). The integration of the coating within the porous architecture enhances its mechanical anchoring, helping resist delamination under physiological loads. Moreover, MBGNs act as a buffering agent, preventing any potential acidification from starch degradation or eugenol oxidation, thereby reducing corrosion risk for Ti-3Cu. The infiltration of bioactive nanoparticles into the pores increases the surface area, which is beneficial for osteoblast attachment and may contribute to faster bone regeneration.<sup>41</sup>

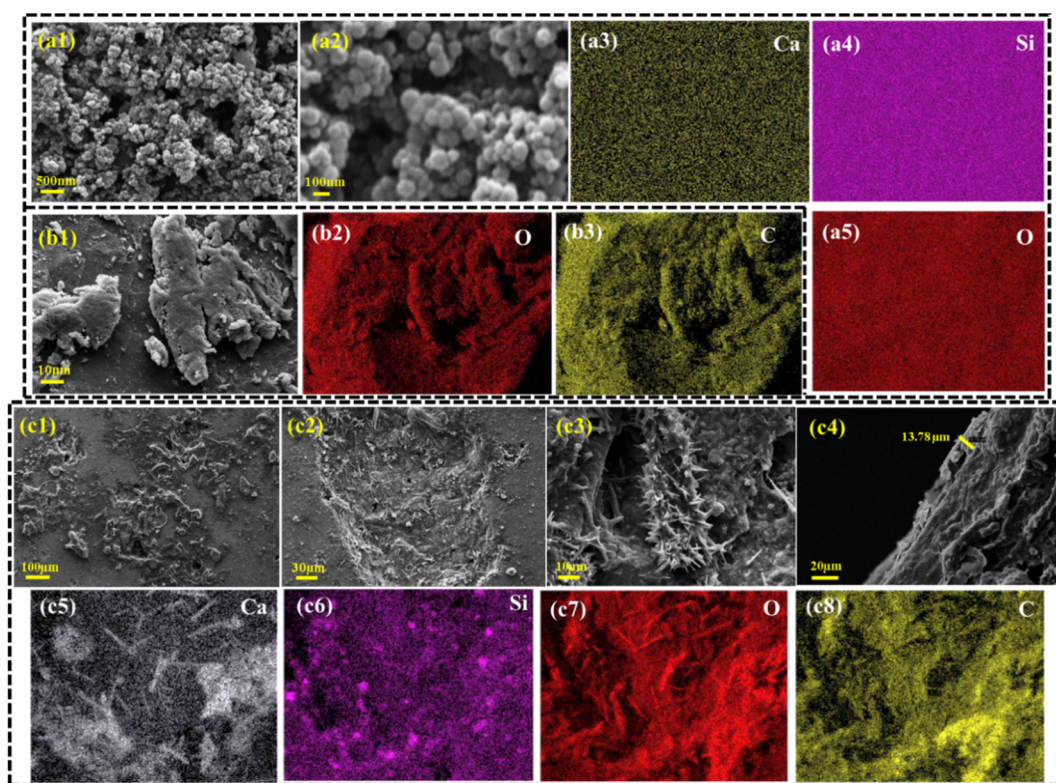


Fig. 4 SEM and elemental analysis performed of MBGNs, (b1–b3) M-starch particles, and (c1–c8) M-starch/MBGNs/clove composite-coated Ti-3Cu substrates.



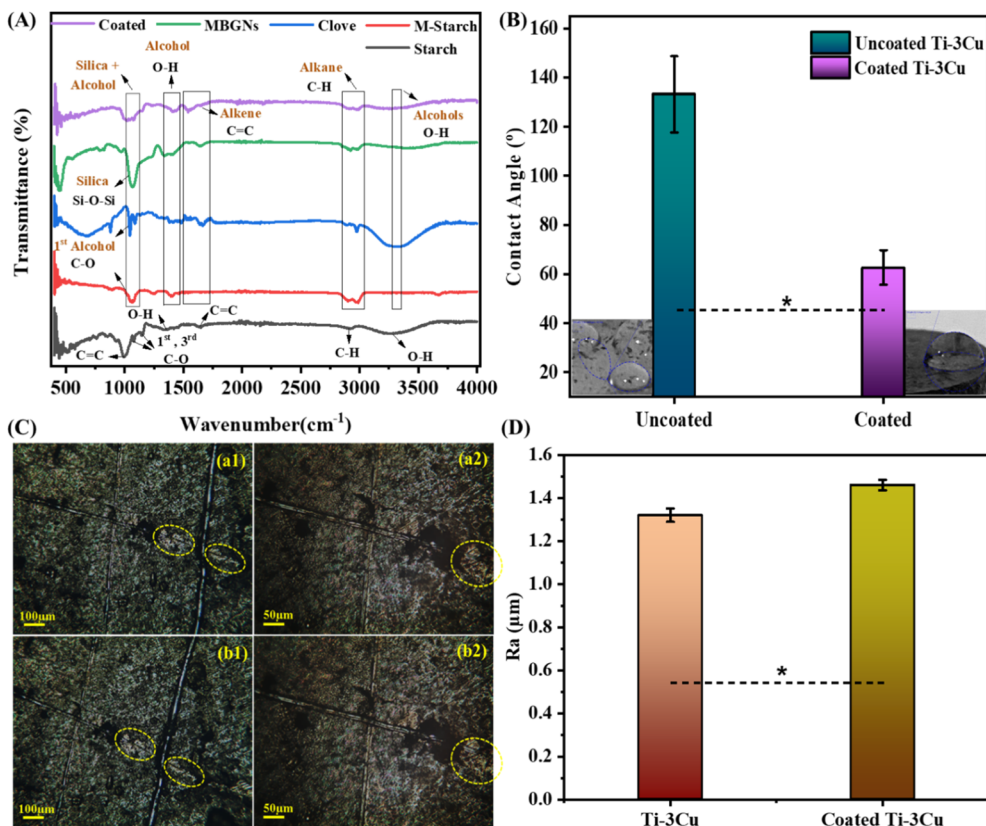


Fig. 5 (A) FTIR spectroscopy, (B) wettability analysis, (C) adhesion testing (a1 and a2) crosshatch test and (b1 and b2) tape test, and (D) surface roughness analysis ( $p < 0.05$ ) of pristine and composite-coated Ti-3Cu substrates.

FTIR analysis was conducted on starch, M-starch, MBGNs, clove, and coated Ti-3Cu substrate (Fig. 5A). The functional groups in starch, particularly alkenes, were converted to alcohol groups in M-starch, a modification crucial for enhancing its

solubility in organic solvents. A broad peak at 1060 cm<sup>-1</sup>, corresponding to silica and alcohol groups, was observed in the coated substrate. This is attributed to the presence of silica groups in MBGNs (peaks at 1041 cm<sup>-1</sup> and 1080 cm<sup>-1</sup>) and

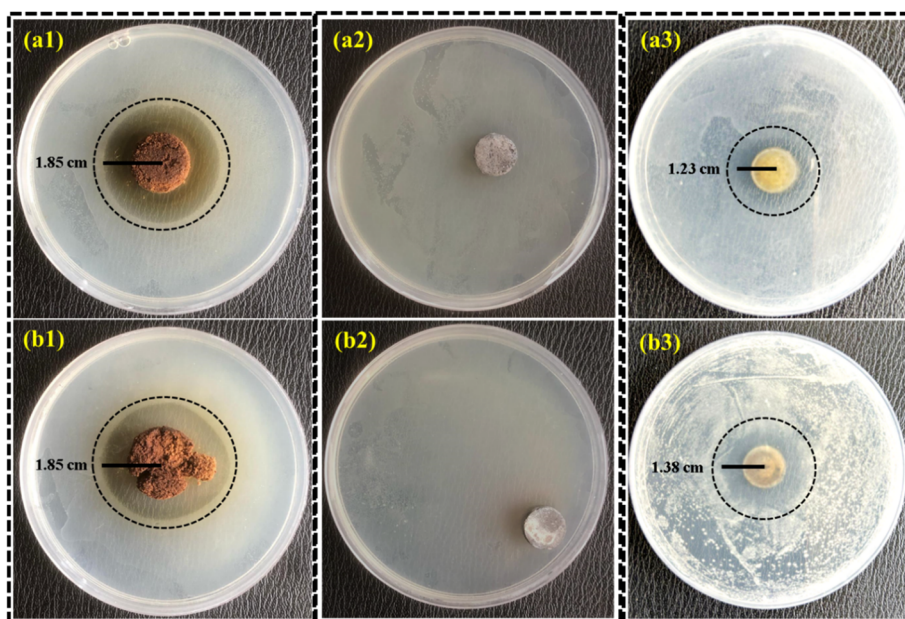


Fig. 6 Antibacterial activity of clove extract, Ti-3Cu substrate, and M-starch/MBGNs/clove extract-coated Ti-3Cu substrate against (a1-a3) *E. coli* and (b1-b3) *S. aureus*, determined through disc diffusion assay.

primary alcohol groups in M-starch and clove (peaks at  $1060\text{ cm}^{-1}$  at  $1067\text{ cm}^{-1}$ , respectively). Additional characteristic peaks were identified at  $1420\text{ cm}^{-1}$  (alcohol groups),  $1540\text{ cm}^{-1}$  and  $1661\text{ cm}^{-1}$  (alkenes), and at  $2910\text{ cm}^{-1}$  and  $2970\text{ cm}^{-1}$  (alkane groups) in the coated particles and substrates. An alcohol group peak at  $3322\text{ cm}^{-1}$  was present in all samples except for M-starch.<sup>42</sup>

The wettability of the synthesized Ti-3Cu substrate sintered at  $750\text{ }^{\circ}\text{C}$  was assessed using the contact angle measurements (Fig. 5B). This is crucial for evaluating surface interactions with biological fluids. The uncoated porous Ti-3Cu substrate exhibited a contact angle of  $133.13^{\circ} \pm 15.51^{\circ}$ , indicating a highly hydrophobic surface. In contrast, after with the MBGNs/M-starch/clove composite, the contact angle decreased significantly to  $62.67^{\circ} \pm 6.98^{\circ}$  (Fig. 5B). This shift reflects a transition from a hydrophobic to a more hydrophilic surface, making it more suitable for orthopedic applications. The differences in wettability of the uncoated bare and coated substrates is particularly important. The hydrophobic surface of uncoated Ti-3Cu substrate can hinder cell adhesion, proliferation, and interaction with surrounding tissues due to repulsion of biological fluids. In contrast, the coated surface, with its increased hydrophilicity, enhances protein adsorption and promotes the adhesion of osteoblasts and other cell.<sup>41</sup> This hydrophilic nature supports osteointegration and osteoconduction, both of which are essential for bone regeneration. Consequently, the modified surface can facilitate faster bone regeneration and contribute to long-term stability of orthopedic implants.<sup>43</sup>

The adhesion of the composite coating deposited on the Ti-3Cu substrate sintered at  $750\text{ }^{\circ}\text{C}$  was evaluated using the crosshatch and tape test, following ASTM D3359 standards. Optical microscope observations revealed that only minimal coating was removed from small areas, with over 95% of the coating remaining intact (Fig. 5C). Based on these results, the coating received a 4B rating, indicating strong adhesion with minimal detachment.<sup>34</sup> High adhesion is particularly important for orthopedic implants, as it ensures the coating remains stable and durable in physiological environments, resisting rapid degradation over time. Strong coating adherence helps maintain the bioactivity and antibacterial properties of the

substrate while promoting effective cell attachment and osteoconduction are key factors for successful bone-implant integration. Additionally, minimal particle detachment reduces the risk of inflammation and implant failure, thereby enhancing the overall safety and effectiveness of the coated Ti-3Cu substrate for orthopedic applications.<sup>44</sup>

High surface roughness is important in orthopedic applications.<sup>45</sup> The average surface roughness ( $R_a$ ) was measured for both uncoated and coated samples (Fig. 5D). The uncoated substrate showed an  $R_a$  value of  $1.32\text{ }\mu\text{m} \pm 0.03\text{ }\mu\text{m}$ , while the coated substrate had a significantly higher value of  $1.46\text{ }\mu\text{m} \pm 0.02\text{ }\mu\text{m}$  ( $p < 0.05$ ). This increase in surface roughness after particle deposition enhances wear resistance and mechanical interlocking, providing more surface area for osteoblast attachment and supporting cell adhesion.<sup>46</sup> Statistical analysis between these two findings shows a significant difference (\*) at  $p < 0.05$ .

### 3.3 Biological properties of M-starch/MBGNs/clove-coated Ti-3Cu substrate

Clove extract has been reported to inhibit bacterial growth.<sup>47</sup> The antibacterial activity of clove, Ti-3Cu substrate, and composite coated Ti-3Cu substrate was evaluated against two common pathogens, the Gram-negative *E. coli* and the Gram-positive *S. aureus*, and the results are presented in Fig. 6 and 7(a). The DDA results showed that for both bacterial strains, clove extract showed the strongest antibacterial activity. In the case of *E. coli* (Fig. 6a1) and *S. aureus* (Fig. 6b1), the inhibition zones were identical, measuring  $1.85\text{ cm}$ , indicating that clove extract is highly effective against both strains. The Ti-3Cu substrate did not show any antibacterial activity against any bacterial strain (Fig. 6a2 and b2), likely due to the low Cu concentration in the alloy, which was insufficient to combat bacterial growth. This confirms that the antibacterial effect in this study originates primarily from clove rather than from copper release, since the low Cu content (3 wt%) does not provide sufficient bactericidal action. Increasing the Cu content could enhance antibacterial activity but must be carefully optimized to cytotoxicity.

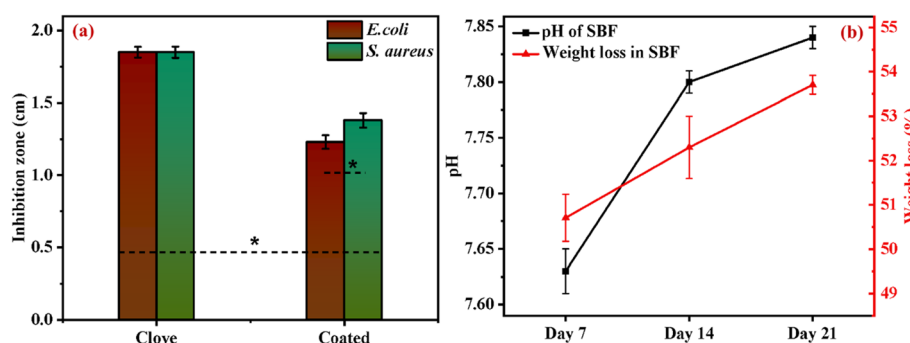


Fig. 7 Statistical analysis of the antibacterial activity of clove and the composite coated sample (a) showed a significant difference (\*) and the difference was significant in *E. coli* and *S. aureus* results of the coated sample. (b) Weight loss of the coating in SBF and changes in the alkalinity of SBF on day 7, 14, and 21.



Antibacterial tests revealed the clove extract tablet produced the largest inhibition zones, while the M-starch/MBGNs/clove-coated Ti-3Cu alloy, in which only 0.1 g clove was used in a 50 mL suspension exhibited moderate inhibition zones of 1.23 cm for *E. coli* (Fig. 6a3) and 1.38 cm for *S. aureus* (Fig. 6b3). This reduction is attributed to a lower absolute clove content and diffusion-limited release of eugenol molecules from the coating matrix, as observed in similar composite coatings. The inhibition zones obtained in this work (1.23–1.38 cm) are consistent with values reported in the literature for polymer-glass-plant extract antibacterial coatings, which typically range between 1.0 and 1.5 cm.<sup>48</sup> The synergistic interaction among starch, MBGNs, and clove ensures sustained antibacterial function: starch provides a hydrophilic and adhesive matrix for

uniform particle dispersion, MBGNs reinforce structural stability and modulate ionic exchange, while clove remains encapsulated within the network to provide controlled antibacterial release. This hybrid configuration prevents rapid volatilization of clove and extends the coating's antibacterial efficacy during the osteointegration period. However, the release of Cu ions is not analyzed in this study.

These results confirm that the composite coating possesses inherent antibacterial properties capable of preventing biofilm formation on orthopedic implants, though it remains less effective than clove extract for both strains. However, the composite coating provides sustained release and reduced risk of cytotoxicity, which is crucial for clinical translation. Antimicrobial activity is critical for an orthopedic applications, as

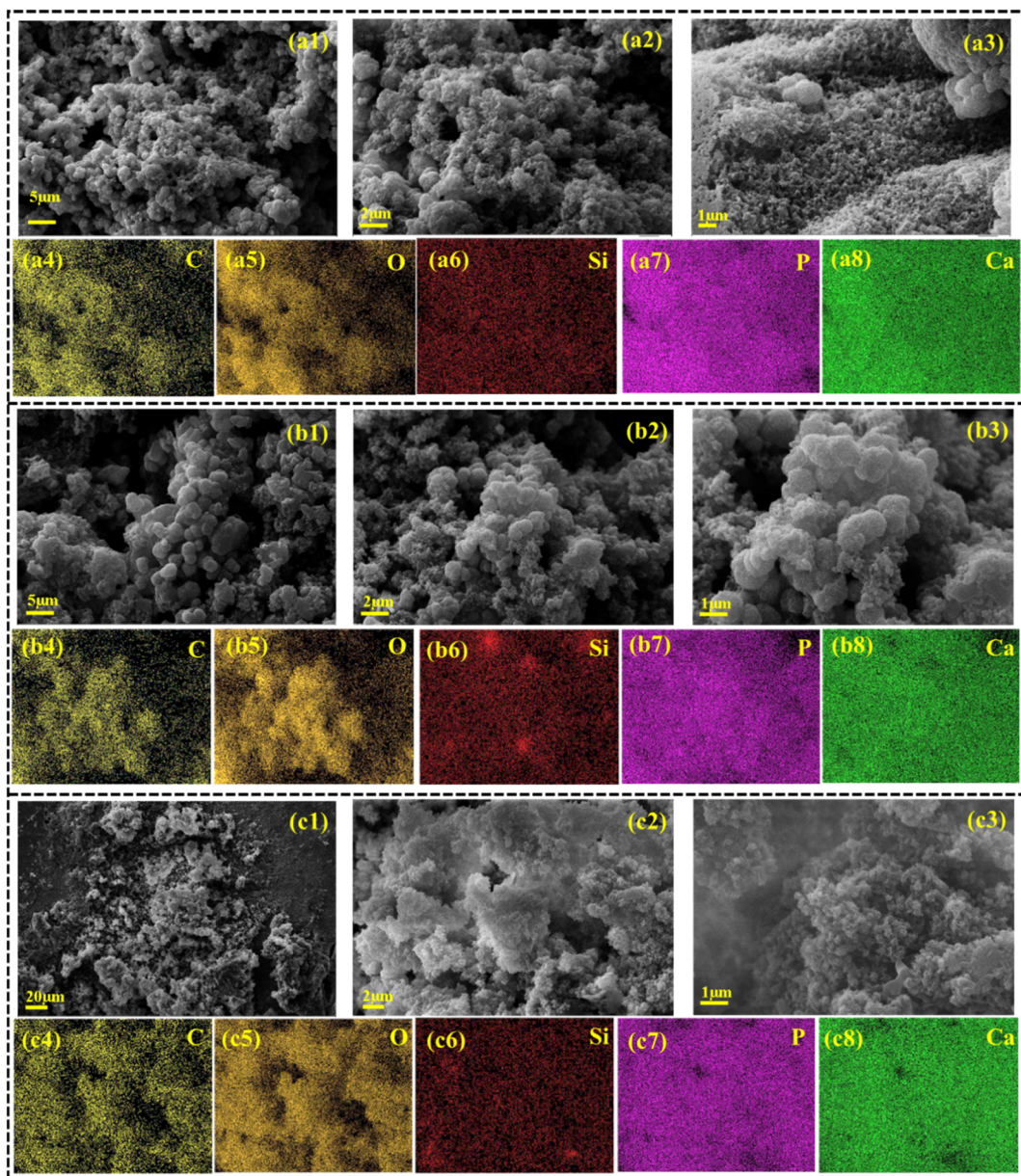


Fig. 8 SEM images and corresponding elemental mappings of the surface morphology and composition of the materials at (a1–a8) day 7, (b1–b8) day 14, and (c1–c8) day 21.



biofilm-associated infections can lead to implant failure.<sup>49</sup> Beyond its antibacterial activity, clove exhibits osteogenic properties that support bone regeneration.<sup>50</sup> This dual functionality enhances the performance of orthopedic implants, improving patient outcomes while minimizing the risk of adverse effects.

The biodegradability of the M-starch/MBGNs/clove composite coating was evaluated by immersing the Ti-3Cu-coated substrate in SBF (pH 7.4) at 37 °C. The degradation rate was relatively fast during the first 7 days, with 50.71% of the coating degraded. This quick degradation is likely due to the swelling behavior of starch and mesoporosity of MBGNs, which allow SBF to penetrate the coating. The degradation rate slowed gradually over time. On day 14, the overall degradation rate was 52.30%, and by day 21, it reached 53.71% (Fig. 7). This stabilization after the initial rapid decline suggests that a significant portion of the coating can be preserved for up to 5–6 weeks, aligning with the typical bone healing period. Therefore, while early degradation promotes bioactive ion release, the remaining coating continues to provide surface bioactivity and stability during the critical osteointegration window. Importantly, the Ti-3Cu alloy substrate itself is biocompatible, ensuring implant safety and functionality even after partial coating loss. For osteointegration, the controlled degradation of the composite coating is advantageous, as it enables the slow release of bioactive elements from the MBGNs, such as Ca, Si, and P ions, which promote bone regeneration. The initial rapid degradation leads to the early release of ions from MBGNs, stimulating osteoblast activity and facilitating implant degradation with surrounding bone tissue, while slower later degradation maintains structural stability for bone healing. Additionally, the inclusion of clove extract, which contains antioxidants, anti-inflammatory, and antimicrobial properties, helps prevent infection and creates a favorable environment for tissue regeneration.<sup>51</sup>

The gradual increase in pH, from 7.63 on day 7 to 7.8 on day 14 and 7.84 on day 21, can be attributed to the release of ions from the MBGNs, particularly Ca and Si ions, which raise the pH. These ions also play a buffering role, stabilizing the local environment and preventing acidic degradation of starch or clove, thereby minimizing any risk of accelerated corrosion of the Ti-3Cu substrate. This shift is beneficial, as a slightly alkaline environment promotes bone mineralization and osteoblastic activity. The final pH value (7.84) remains within the physiological tolerance range (7.2–8.0), indicating that the coating does not induce cytotoxic alkalinity but rather supports osteoblastic proliferation and HA formation. Therefore, the pH increase not only supports bone formation but also indicates positive interaction between the coating and the biological environment which supports osteoblastic activity by creating a slightly alkaline environment, making it ideal for long-term orthopedic implant applications.<sup>52</sup>

Bioactivity is critical for preventing white blood cells from treating implants as foreign agents and for promoting osteoblast attachment to the substrate surface. The bioactivity of M-starch/MBGNs/clove-coated composite on Ti-3Cu substrate was studied over 7, 14, and 21 days in SBF.<sup>53</sup> SEM images revealed

changes in morphology over time. On day 7 (Fig. 8a1–a3), the hydroxyapatite (HA) layer began to form across the substrate, although it was more prominent in certain areas. By day 14 (Fig. 8b1–b3), the HA layer had grown and became more distinct at microstructural level. By day 21 (Fig. 8c1–c3), the surface was almost entirely covered by the HA layer, demonstrating consistent and progressive bioactivity promoted by composite coating.<sup>54</sup> The gradual growth of the HA layer highlights the ability of the coating to integrate with the bone tissue, promoting long-term stability and implant integration with the surrounding bone.<sup>55</sup> As the HA layer develops on the substrate surface, it provides a cell-stimulating surface that facilitates osteoblast adhesion, proliferation, and differentiation, supporting bone regeneration.<sup>56</sup> Elemental analysis confirmed the formation of the HA layer, evidenced by the presence of calcium–phosphate (Ca/P), along with Si, C, and O (Fig. 8a4–a8, b4–b8 and c4–c8). These results are in accordance with a previous study.<sup>57</sup> The Ca/P ratio was 1.25 on day 7 with an initial formation of the HA layer. This ratio increased to 1.35 on day 14 due to the continued mineralization, and further rose to 1.51 on day 21, which, although close to the Ca/P ratio of tricalcium phosphate, remains below the stoichiometric HA ratio of ~1.67. Therefore, the results indicate progressive bone-like apatite formation rather than fully stoichiometric HA. The increment in the Ca/P ratio suggests that the implant surface not only exhibits bioactivity but also forms a stable and progressively mineralized apatite layer, which supports osteointegration in orthopedic applications.<sup>58</sup>

*In vitro* cellular studies were performed on day 1, 3, 5, and 7 to assess the cell viability of both uncoated Ti-3Cu and composite-coated Ti-3Cu substrates. The cell viability of the control sample was  $29.27 \pm 1.11\%$  on day 1,  $50.85 \pm 0.95\%$  on day 3,  $68.16 \pm 1.2\%$  on day 5, and 100% on day 7, which served as the reference for comparison. For the uncoated substrate, cell viability started at  $20.1 \pm 2.52\%$  on day 1, increasing to  $39.31 \pm 3.8\%$  on day 3 and  $63.25 \pm 2.2\%$  on day 5. By day 7, cell viability reached  $94.66 \pm 1.88\%$  (Fig. 9). These lower cell

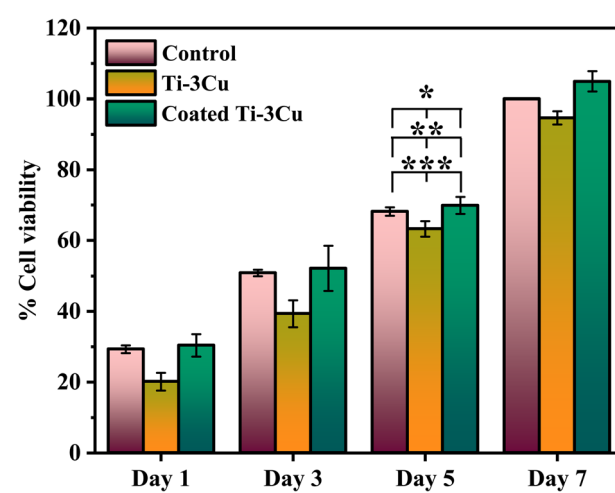


Fig. 9 Cell viability on uncoated Ti-3Cu and M-starch/MBGNs/clove-coated composite substrates at different time points.  $p < 0.05$  (\*),  $p < 0.01$  (\*\*), and  $p < 0.001$  (\*\*\*)



viability rates, compared to the control, can be attributed to the hydrophobic nature and low surface roughness of the substrate.<sup>52</sup> In contrast, the composite-coated Ti-3Cu substrate exhibited significantly higher cell viability. On day 1,  $30.34 \pm 3.17\%$  cells survived, while  $52.14 \pm 6.35\%$  cells survived on day 3. By day 5, cell viability was  $69.87 \pm 2.42\%$ , and on day 7, it reached  $104.91 \pm 2.87\%$  (Fig. 9), interpreted as enhanced proliferation compared to 316L SS baseline, with statistical significance reported ( $p < 0.05$ ). These results indicate that the coating was non-toxic and supported cell attachment and proliferation.<sup>59</sup> Additionally, the hydrophilic nature and increased surface roughness of the composite coating contributed to its osteoconductivity promoting cell attachment.<sup>60</sup>

## 4. Conclusions

In conclusion, the development of Ti-3Cu porous alloys with bioactive composite coatings represents a significant advancement in the field of orthopedic implants. By optimizing the sintering process at  $750\text{ }^{\circ}\text{C}$ , the Ti-3Cu alloys achieved a balanced combination of mechanical strength and porosity, making them suitable for broad-range applications in bone and joint repair. This optimization is particularly important because it prevents stress shielding while maintaining sufficient load-bearing capacity, highlighting the metallurgical contribution of controlled  $\text{Ti}_2\text{Cu}$  phase formation and tailored porosity. The addition of a bioactive coating, consisting of M-starch, MBGNs, and clove particles, sequentially enhanced the surface properties of the alloy. The coating improved the surface wettability, reducing the contact angle and promoting better adhesion, which is critical for cell attachment and subsequent osseointegration. Furthermore, the composite coating exhibited antibacterial activity against common pathogens such as *E. coli* and *S. aureus*, thus reducing the risk of implant-related infections. The bioactivity of the coated alloys was confirmed by the progressive formation of HA in SBF, a key indicator of bone regeneration potential. Biodegradability tests showed controlled degradation of the coating, which releases bioactive ions that support osteoblast activity and enhance bone healing. The cytocompatibility assay further confirmed the enhanced cell viability on the composite-coated substrates, indicating a stimulatory effect on osteoblast proliferation. This dual action of supporting bone healing while minimizing infection risk highlights the biomedical significance of the starch/MBGNs/clove coating. Overall, Ti-3Cu alloys with bioactive coatings offer a promising solution for improving the performance and durability of orthopedic implants, by integrating metallurgical optimization with multifunctional surface bioactivity to enhance osseointegration, infection resistance, and long-term stability.

## Conflicts of interest

The authors declare that they have no known competing financial interests or personal relationships that could have appeared to influence the work reported in this paper.

## Data availability

The data that supports the findings of this study are available from the first author upon reasonable request.

## Acknowledgements

M. A. Marwat acknowledges the valuable academic and research support from Pakistan Science Foundation Project No. PSF-NSFC/202307/19 and Ghulam Ishaq Khan (GIK) Institute of Engineering Sciences and Technology.

## References

- 1 J. Gong, J. Liu, X. Song, Y. Li, Y. Wang and Z. Chen, *J. Alloys Compd.*, 2024, **995**, 174823.
- 2 Y. Zhao, Q. Wu, H. Zhou, C. Zhao and L. Wu, *J. Alloys Compd.*, 2024, **977**, 173419.
- 3 P. Du, B. Zhu, X. Yang and G. Xie, *J. Alloys Compd.*, 2021, **886**, 161290.
- 4 L. Zhang, Z. Y. He, J. Tan, M. Calin, K. G. Prashanth, B. Sarac, B. Völker, Y. H. Jiang, R. Zhou and J. Eckert, *J. Alloys Compd.*, 2017, **727**, 338–345.
- 5 E. B. Taddei, V. A. R. Henriques, C. R. M. Silva and C. A. A. Cairo, *Mater. Sci. Eng., C*, 2004, **24**, 683–687.
- 6 F. Guillemot, *Expert Rev. Med. Devices*, 2005, **2**, 741–748.
- 7 S. M. Javadhesari, S. Alipour and M. Akbarpour, *Colloids Surf., B*, 2020, **189**, 110889.
- 8 E. Zhang, X. Wang, M. Chen and B. Hou, *Mater. Sci. Eng., C*, 2016, **69**, 1210–1221.
- 9 E. Zhang, L. Zheng, J. Liu, B. Bai and C. Liu, *Mater. Sci. Eng., C*, 2015, **46**, 148–157.
- 10 H.-L. Yang, L. Zou, A. N. Juaim, C.-X. Ma, M.-Z. Zhu, F. Xu, X.-N. Chen, Y.-Z. Wang and X.-W. Zhou, *Rare Met.*, 2023, **42**, 2007–2019.
- 11 M. Bao, Y. Liu, X. Wang, L. Yang, S. Li, J. Ren, G. Qin and E. Zhang, *Bioact. Mater.*, 2018, **3**, 28–38.
- 12 S. C. Mendes, R. Reis, Y. P. Bovell, A. Cunha, C. A. van Blitterswijk and J. D. de Bruijn, *Biomaterials*, 2001, **22**, 2057–2064.
- 13 C. Yi, Z. Ke, L. Zhang, J. Tan, Y. Jiang and Z. He, *Mater. Res. Express*, 2020, **7**, 105404.
- 14 J. Liu, X. Zhang, H. Wang, F. Li, M. Li, K. Yang and E. Zhang, *Biomed. Mater.*, 2014, **9**, 025013.
- 15 S. Tao, J. Xu, L. Yuan, J. Luo and Y. Zheng, *J. Alloys Compd.*, 2020, **812**, 152142.
- 16 S. Prabakaran, M. Rajan, Z. Geng and Y. Liu, *Carbohydr. Polym.*, 2021, **271**, 118432.
- 17 R. Aqib, S. Kiani, S. Bano, A. Wadood and M. A. Ur Rehman, *Int. J. Appl. Ceram. Technol.*, 2021, **18**, 544–562.
- 18 F. Maciąg, T. Moskalewicz, K. Cholewa-Kowalska, Z. Hadzhiieva, M. Dziadek, B. Dubiel, A. Łukaszczuk and A. Boccaccini, *J. Electrochem. Soc.*, 2023, **170**, 082501.
- 19 I. Unalan and A. R. Boccaccini, *Curr. Opin. Biomed. Eng.*, 2021, **17**, 100261.



20 K. Ahmad, J. Manzur, M. Tahir, R. Hussain, M. Khan, A. Wadood, E. Avcu and M. A. U. Rehman, *Prog. Org. Coat.*, 2023, **176**, 107407.

21 D. M. Marques, V. d. C. Oliveira, M. T. Souza, E. D. Zanotto, J. P. M. Issa and E. Watanabe, *Biofouling*, 2020, **36**, 234–244.

22 R. Sinha and R. Tuan, *Bone*, 1996, **18**, 451–457.

23 A. Bandyopadhyay, I. Mitra, S. Ciliveri, J. D. Avila, W. Dernell, S. B. Goodman and S. Bose, *Int. J. Extrem. Manuf.*, 2023, **6**, 015503.

24 W. Li and D. Zhao, *Adv. Mater.*, 2013, **25**, 142–149.

25 J.-P. Wang, S.-J. Yuan, Y. Wang and H.-Q. Yu, *Water Res.*, 2013, **47**, 2643–2648.

26 S. A. Batool, K. Ahmad, M. Irfan and M. A. Ur Rehman, *J. Funct. Biomater.*, 2022, **13**, 97.

27 L. Besra and M. Liu, *Prog. Mater. Sci.*, 2007, **52**, 1–61.

28 M. A. Marwat, M. F. Khan, M. Humayun, S. Ali, M. R. A. Karim, S. S. Shah, M. Bououdina, Z. U. Din, K. M. Adam and S. M. Abdullah, *Electrochim. Acta*, 2025, **511**, 145373.

29 U. Hamayun, M. A. Marwat, S. M. Abdullah, R. Ullah, M. Humayun, M. Bououdina, M. R. A. Karim, M. Z. Khan and M. B. Hanif, *J. Alloys Compd.*, 2024, 178422.

30 M. A. Marwat, S. Ishfaq, K. M. Adam, B. Tahir, M. H. Shaikh, M. F. Khan, M. R. A. Karim, Z. U. Din, S. Abdullah and E. Ghazanfar, *RSC Adv.*, 2024, **14**, 2102–2115.

31 M. A. Marwat, H. Zhang, M. Humayun, B. Xie, M. Ashtar, M. Bououdina, M. U. Rehman and S. Ishfaq, *J. Energy Storage*, 2024, **79**, 110125.

32 E. Ghazanfar, M. A. Marwat, S. A. Batool, A. Anwar, S. M. Abdullah, Z. U. Din, M. Humayun, M. Bououdina, A.-B. Abo-Elnasr and H. T. Ali, *RSC Adv.*, 2024, **14**, 26775–26787.

33 I. De-la-Pinta, M. Cobos, J. Ibarretxe, E. Montoya, E. Eraso, T. Guraya and G. Quindós, *J. Mater. Sci.: Mater. Med.*, 2019, **30**, 1–11.

34 C. Magdaleno-López and J. de Jesús Pérez-Bueno, *Int. J. Adhesion Adhes.*, 2020, **98**, 102551.

35 M. E. McKnight, J. F. Seiler, T. Nguyen and W. J. Rossiter, *J. Prot. Coat. Linings*, 1995, **12**, 82.

36 T. Kokubo and H. Takadama, *Biomaterials*, 2006, **27**, 2907–2915.

37 C. Pautke, M. Schieker, T. Tischer, A. Kolk, P. Neth, W. Mutschler and S. Milz, *Anticancer Res.*, 2004, **24**, 3743–3748.

38 W. Akram, R. Khan, M. Petru, M. Amjad, K. Ahmad, M. Yasir, S. Ahmad and S. S. R. Koloor, *J. Mater. Res. Technol.*, 2023, **26**, 2587–2600.

39 K. Präbst, H. Engelhardt, S. Ringgeler and H. Hübner, *Cell viability assays: methods and protocols*, Springer New York, New York, NY, 2017, pp. 1–17.

40 R. N. Elshaer and K. M. Ibrahim, *Trans. Nonferrous Metals Soc. China*, 2020, **30**, 1290–1299.

41 Y. Yang, R. Cavin and J. L. Ong, *J. Biomed. Mater. Res., Part A*, 2003, **67**, 344–349.

42 D. L. Pavia, G. M. Lampman, G. S. Kriz and J. R. Vyvyan, *SERBIULA (sistema Librum 2.0)*, 2015.

43 T. Kustos, I. Kustos, F. Kilár, G. Rappai and B. Kocsis, *Cancer Chemotherapy*, 2003, **49**, 237–242.

44 Y. Zaokari, A. Persaud and A. Ibrahim, *Eng. Regen.*, 2020, **1**, 51–63.

45 S. Swain and T. R. Rautray, *Nanostructured Materials Their Applications*, 2021, pp. 55–80.

46 L. Li, K. Crosby, M. Sawicki, L. L. Shaw and Y. Wang, *J. Biotechnol. Biomater.*, 2012, **2(06)**, 1000150.

47 S. Saeed and P. Tariq, *Pak. J. Bot.*, 2008, **40**, 2157–2160.

48 B. F. Adamu, J. Gao, S. Tan and E. K. Gebeyehu, *J. Ind. Text.*, 2022, **51**, 1793S–1814S.

49 B. H. Abdullah, S. F. Hatem and W. Jumaa, *Pharm. Biosci. J.*, 2015, 18–22.

50 M. F. A. El-Maati, S. A. Mahgoub, S. M. Labib, A. M. Al-Gaby and M. F. Ramadan, *Eur. J. Integr. Med.*, 2016, **8**, 494–504.

51 M. M. Saleh, A. Touny, M. A. Al-Omair and M. Saleh, *Bio-Med. Mater. Eng.*, 2016, **27**, 87–99.

52 D. A. Puleo, L. A. Holleran, R. H. Doremus and R. Bizios, *J. Biomed. Mater. Res.*, 1991, **25**, 711–723.

53 J. Liang, X. Lu, X. Zheng, Y. R. Li, X. Geng, K. Sun, H. Cai, Q. Jia, H. B. Jiang and K. Liu, *Front. Bioeng. Biotechnol.*, 2023, **11**, 1269223.

54 J. R. Jones, D. S. Brauer, L. Hupa and D. C. Greenspan, *Int. J. Appl. Glass Sci.*, 2016, **7**, 423–434.

55 J. Ajita, S. Saravanan and N. Selvamurugan, *Mater. Sci. Eng., C*, 2015, **53**, 142–149.

56 Z. Qu, X. Rausch-Fan, M. Wieland, M. Matejka and A. Schedle, *J. Biomed. Mater. Res., Part A*, 2007, **82**, 658–668.

57 S. Lopez-Esteban, E. Saiz, S. Fujino, T. Oku, K. Saganuma and A. P. Tomsia, *J. Eur. Ceram. Soc.*, 2003, **23**, 2921–2930.

58 F. Tan, M. Naciri and M. Al-Rubeai, *Biotechnol. Bioeng.*, 2011, **108**, 454–464.

59 K. Anselme, *Biomaterials*, 2000, **21**, 667–681.

60 A. Hunter, C. Archer, P. Walker and G. Blunn, *Biomaterials*, 1995, **16**, 287–295.

